Solute distribution in the ferromagnetic matrix of an M50 high-speed steel in annealed and quenched states

1997 J. Phys.: Condens. Matter 9 4931

(http://iopscience.iop.org/0953-8984/9/23/017)

J. Phys.: Condens. Matter **9** (1997) 4931–4942. Printed in the UK PII: S0953-8984(97)77803-2

Solute distribution in the ferromagnetic matrix of an M50 high-speed steel in annealed and quenched states

C Djega-Mariadassou†, B Decaudin†, L Bessais‡ and G Cizeron†

† Laboratoire de Structure des Matériaux Métalliques, Bâtiment 414, Université de Paris Sud, 91405 Orsay Cédex, France

‡ Groupe de Physique des Solides, Paris 7 et Paris 6, Tour 23, 2 Place Jussieu, 75251 Paris Cédex 05, France

Received 13 September 1996, in final form 25 November 1996

Abstract. A method of analysing by Mössbauer spectroscopy a steel ferromagnetic matrix has been developed. It provides the fractions of atomic elements in substitutional or interstitial sites in the Fe lattice, from the comparison between the experimental hyperfine-field distribution $P(H)_{exp}$ and the calculated one $P(H)_{cal}$. This method, applied to an M50 steel, in the simple case of ferrite (the annealed state), and extended to the most complex situation of martensites quenched from various temperatures, describes the initial state of the steel before any further tempering treatment. The atomic fractions of Cr, Mo, V, and C in the Fe lattice have been specified.

1. Introduction

High-speed steels can be classified, according to their composition, into two groups: those enriched in W, and those for which Mo is substituted for W. A special category of these latter alloys, where W is totally replaced by Mo, have been developed in order to avoid the use of the expensive element W. They cannot be considered as a good substitute for the usual high-speed steels if small grain size and good properties of hardness after tempering are required: they show a high tendency towards grain coarsening, so the choice of their austenizing temperature is critical, as it must represent a balance between the carbide dissolution rate, the amount of austenite retained, and the grain size. Moreover, they can decarburize easily, and must be annealed under vacuum or in salt baths.

The category of the completely Mo-alloyed steels present some of the characteristics of the W high-speed steels: high hardness after tempering, and wear resistance with good toughness. They contain 4 wt% of Cr, like the classical high-speed steels. Since their Mo content is much lower than the W content in the W high-speed steels, it is balanced by high V and C contents: they commonly show around 2 wt% of V combined as MC-type carbides (M = Fe, Mo, V, Cr). The M50 steel (or 80DCV40) which is the steel used in the present study is a special case, because its V content is around 1 wt%, and its Mo content around 4 wt%. This steel, widely used in aeronautics, is used at temperatures between 150 and 300 °C.

A clear understanding of its microstructural changes under various heat treatments, which would lead to secondary hardening precipitation by means of finely dispersed carbides, is therefore important if one is to optimize its lifetime.

0953-8984/97/234931+12$19.50

The analysis of precipitates [1] distributed in the matrix requires lengthy procedures and the combination of different techniques, such as x-ray diffraction, transmission electron microscopy, and x-ray microprobe analysis. As their volume fraction is around 10%, it is easier to study them using measurements after electrolytic extraction. An interesting contribution to the knowledge of the hardening process can be provided indirectly by Mössbauer spectroscopy. More particularly, a comparison of the ferromagnetic matrix in the ferritic state with that of the martensites intended to undergo subsequent tempering treatments can represent a good basis for controlling the initial step of the precipitation. Moreover, Mössbauer spectroscopy gives a good statistical representation of the samples. In this work, transmission Mössbauer spectroscopy was carried out at 300 K to obtain the magnetic hyperfine-field distribution $P(H)$ of the ferritic and the various martensitic matrices. The subsequent modifications of the Mössbauer spectra, indicative of the martensitic matrix disturbances as detected by the evolution of $P(H)$, will be compared to simulated hyperfine-field distributions according to our method established for modelling ternary Fe–Ni–Mo alloys with substituted elements [2]. The purpose of this paper is to extend this method to more complex situations: the ferritic state for which the substitution leads to the quaternary system Fe–Cr–Mo–V, and the martensitic states which, at the same time, depend on substitutional and interstitial sites in the Fe lattice.

2. Experimental procedures

The chemical composition of commercially available M50 steel, which is in the annealed state, is given in table 1. The alloying elements which have to be taken into account are Mo, Cr, and V. The elements Si, Mn, and Ni can be treated as dispersed impurities, and will not influence the observed tendencies of the Mössbauer spectra.

Table 1. The chemical composition of commercial M50 steel.

	Fe	C	Mo	Cr	V	Si	Mn	Ni
wt%	Base	0.88	3.97	4.15	1.03	0.29	0.26	0.080
at.%	Base	4.02	2.27	4.37	1.11	0.57	0.20	0.075

The ferrite was obtained by annealing the as-received sample for five hours at 1073 K to eliminate any residual austenite. The samples were subsequently cooled at a rate of 0.2 K s^{-1}. The quenched states were obtained after submitting the annealed state to austenizing treatments at various temperatures, $\Theta\gamma$, of 1273 K, 1373 K, and 1423 K for five minutes, before water quenching at 50 K s^{-1}.

To test the disturbances caused by Cr, Mo, and V at the Fe nuclei, several disordered binary alloys, $Fe_{1-x}M_x$ (M = Cr, Mo, V), were prepared with compositions close to those of the steel, from high-purity powders, with sintering temperatures of 1475–1575 K, for 12 hours in a hydrogen atmosphere. They were laminated to 100 μm, and finally annealed at 1120 K and quenched in air at 15 K s^{-1}. Their overall composition was determined from x-ray microprobe analysis (see table 2).

For the Mössbauer experiments, the samples were thinned down to 15 μm to eliminate any absorption correction. For that purpose, a chemical treatment with a solution of HF and H_2O_2 was preferred to a mechanical reduction, so as to avoid any disturbance which could occur due to retained austenite in martensitic samples.

The Mössbauer spectra were collected at room temperature with a conventional constant-

Table 2. The chemical compositions of the binary alloys, from x-ray microprobe analysis (in atomic per cent).

$Fe_{1-x}M_x$	M = Cr	M = Mo	M = V
x	0.020 ± 0.002	0.012 ± 0.001	0.003 ± 0.002
x	0.054 ± 0.005	0.031 ± 0.002	0.014 ± 0.001

acceleration 512-channel spectrometer in transmission geometry, operating in the mirror-image mode with a 50 mCi γ-source for ^{57}Co in a Rh matrix. A small linear drift of the base-line was corrected. The α-Fe reference had a linewidth of 0.25 mm s^{-1} for the outermost peaks. The spectra were analysed according to two procedures. They were first decomposed into broadened discrete subspectra by means of a least-squares fit to lorentzian lines. The resulting relationships between the isomer shift δ, quadrupole splitting ε, and magnetic hyperfine field H were used in a second step to extract the experimental hyperfine-field distribution $P(H)_{exp}$ with an improved version of the Hesse and Rubartsch method, where H-values are large with respect to the electric field gradient [3]. The linewidth of each site was quoted as equal to 0.25 mm s^{-1}.

3. Simulation of the magnetic hyperfine-field distribution $P(H)$

The principle of the $P(H)$ calculation, limited to the configuration probability calculations for the first two neighbouring shells of an iron nucleus, will be briefly recalled [2]. However, as steels are multi-component, with solute atoms in substitutional and (or) in interstitial sites in the Fe lattice, we shall then report the probability calculations in both cases, and subsequently define the field disturbance, $\Delta H_{k,i}$, experienced by one Fe nucleus surrounded by solutes of an element k, in the ith coordination shell.

3.1. General method

In the concept of additive effects of the neighbour disturbances in dilute binary alloys, the magnetic hyperfine field H of an iron nucleus in a b.c.c. lattice with randomly distributed solutes can be expressed as

$$H = H_0 + \sum_{i=1}^{2} n_i \, \Delta H_i .$$

H_0 corresponds to the magnetic hyperfine field of pure iron, and n_i represents the number of solute atoms in the coordination sphere i around one iron nucleus leading to a configuration α_i. ΔH_i is the hyperfine-field increment corresponding to the ith coordination sphere disturbing the iron nucleus.

In a first step, the first two coordination shells will be considered, neglecting the effects of the higher shells.

With the assumption of independent effects of the various surrounding atoms located on the first two shells, α being the combined configuration $\alpha = \{\alpha_1, \alpha_2\}$, the total probability $P(\alpha)$, of the configuration α_i is

$$P(\alpha) = \prod_{i=1}^{2} P(\alpha_i).$$

The resulting hyperfine field $H(\alpha)$ for alloying element k distributed on the ith shell can be written as

$$H(\alpha) = H_0 + \sum_{i=1}^{2} \sum_{k=1}^{K} n_{k,i}\, \Delta H_{k,i}.$$

$n_{k,i}$ is the number of atoms of species k in sphere i, and $\Delta H_{k,i}$ is the field increment associated with $n_{k,i}$.

We should take into account the effects of the atoms located on the higher shells, but these effects decrease when the solutes are more distant. Consequently these effects will be taken as random variables, and the central-limit theorem rules that their asymptotic behaviour is a gaussian function G with zero mean and finite variance σ: $G(0, \sigma)$. It thus follows that a realistic representation of the magnetic hyperfine field will be given by the convolution of the hyperfine-field distribution, provided by the probability $P(\alpha)$ including the first two coordination shells, with a gaussian distribution of the disturbing effects identifiable with a hyperfine field H_D caused by the more distant shells.

The resulting calculated probability $P(H)_{cal}$ will now be expressed as

$$P(H)_{cal} = P(H(\alpha))P(H_D)$$

where $P(H(\alpha))$ is the probability of the field $H(\alpha)$ in the configuration α, and $P(H_D)$ is the probability of the disturbing field H_D equal to $G(0, \sigma)$.

The adjustable parameters governing the calculation of the magnetic hyperfine-field distribution are the alloy composition, which determines $P(\alpha)$, the field increments $\Delta H_{k,i}$ relating to the element k on the ith coordination sphere either in substitution or in insertion, and the variance σ of the gaussian function involving the effects of the higher shells. The minimum R-value is connected to the best agreement between the experimental distribution $P(H)_{exp}$ extracted from the Mössbauer spectra and the simulated one $P(H)_{cal}$, and is defined as

$$R = \left[\left(\sum_j (P_j(H)_{cal} - P_j(H)_{exp})^2 \right) \Big/ N \right]^{1/2}.$$

$P_j(H_{cal})$ and $P_j(H_{exp})$ represent respectively the theoretical and the experimental distributions deduced from the experimental data, where N is the number of experimental points.

3.2. Probability calculations for the two first coordination shells of one Fe atom

The metallic alloying species k in disordered alloys are located on substitutional positions. Let us write P_{sub} for the probability $P(\alpha)$ of a given configuration α_1, α_2 in the particular case of substitution. P_{sub} obeys the multinomial law

$$P_{sub} = \prod_{i=1}^{2} \left[N_i! \Big/ \prod_{k=0}^{K} n_{k,i}! \right] \prod_{k=0}^{K} p_k^{n_{k,i}}.$$

N_i is the total number of neighbours in shell i: $N_i = 8$ for $i = 1$ and $N_i = 6$ for $i = 2$ in a b.c.c. lattice. $n_{k,i}$ is the number of neighbours of species k in shell i for given configurations α_1, α_2, and varies from 1 to 8 for $i = 1$ and from 1 to 6 for $i = 2$. p_k is the atomic fraction of the alloying element k, so

$$\sum_{k=0}^{K} p_k = 1.$$

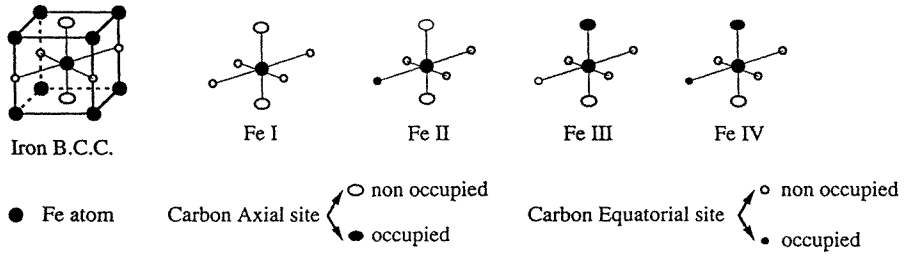

Figure 1. The various Fe species corresponding to the octahedral sites located in a direction parallel to the [001] axis (O_c).

Table 3. The interstitial site probabilities P_{int} for FeC_x compounds, on the assumption of a statistical distribution of the C atoms in the octahedral sites located along the ⟨001⟩ direction.

Iron species	Number of first neighbours	Number of second neighbours	P_{int}
Fe I	0	0	$(1-x)^6$
Fe II	0	1	$4x(1-x)^5$
Fe III	1	0	$2x(1-x)^5$
Fe IV	1	1	$8x^2(1-x)^4$

Table 4. The abundance (A) of the Mössbauer experimental subspectra of FeC_x compounds ($0 < x \leqslant 0.05$) [4], and the theoretical probabilities P_{int}, on the assumption of a statistical distribution of C atoms in the octahedral sites located along the ⟨001⟩ direction.

				P_{int} (%)				
x		A (%)		Fe I	Fe II	Fe III	Fe IV	$\sum$
0.02	89.9	6.9	3.2	88.58	7.23	3.61	0.29	99.71
0.03	84.6	9.9	5.5	83.29	10.30	5.15	0.63	99.37
0.04	78.5	14	7.6	78.27	13.58	6.79	1.08	99.72
0.05	71.7	18	10.3	73.50	15.47	7.73	1.63	98.32

In the case of carbon interstitials which involve the low-dilution range ($x \leqslant 0.05$), the site occupation can be considered as random, but within the limits imposed by the crystallographic tetragonal distortion. Among the six octahedral sites, the occupied sites are those lying in a direction parallel to the [001] axis (O_c). They are the axial sites located at $c/2$ from an iron atom, and correspond to the first neighbours of an Fe atom, because for $c/a = 1.03$, $c/2$ is always shorter than $a\sqrt{2}/2$, the distance which characterizes the second coordination sphere. Among the 12 octahedral sites, only the four sites in the plane perpendicular to the [001] axis containing the central Fe atom are occupied. These are the equatorial sites (figure 1).

The main configurations describing the interstitial neighbourhood of an iron atom are directly connected to the interstitial probabilities P_{int} given in table 3 for FeC_x alloys.

The interesting x-values are limited to $x = 0.05$, as they deal with the maximum C content consistent with the M50 steel composition. It appears that four Fe configurations at most can be observed on the experimental Mössbauer spectra, assuming a random

distribution of interstitial elements with $x \leqslant 0.05$, as shown by the calculated P_{int}-values reported in table 4.

$P_{1,1}$ might still be neglected, and this is all the more so for $P_{0,2}$ which is eight times lower than $P_{1,1}$. For steels, the ferritic state will only be affected by substitution, whereas the martensitic states will involve both substitutional and interstitial sites, so the resulting probability for a given configuration will be the product $P_{sub}P_{int}$.

4. Results and discussion

4.1. Determinations of the field increments $\Delta H_{k,i}$

The known values of the increments $\Delta H_{k,i}$ ($k =$ Cr, Mo, V; $i = 1, 2$) were obtained from binary $Fe_{1-x}M_x$ alloys for low solute contents [5–10] (see table 5).

Table 5. $\Delta H_{k,i}$ values from previous work; dashes indicate that values were not given by the authors. The accuracy was not given by authors, except in reference [5].

	Percentage atomic substitution	$\Delta H_{k,1}$ (kOe)	$\Delta H_{k,2}$ (kOe)
Fe–Cr	— [6]	−28	−24
	4.8 [7, 8]	−34.5	−24
	2.2 [5]	−26.9 (0.2)	−26.9 (0.2)
Fe–V	4–16 [6]	−26	−22
	— [9]	−24	−24
	2–5 [5]	−24.3 (0.2)	−24.3 (0.2)
Fe–Mo	3.2 [10]	−37	−18
	1.0 [5]	−38.7 (0.5)	−31.6 (0.7)

Table 6. Evaluations of the compositions, x, and increment fields, $\Delta H_{k,i}$, for the synthesized $Fe_{1-x}M_x$ alloys.

	Composition x				
Alloy	X-ray microanalysis	HFD (±0.002) simulation	$\Delta H_{k,1}$ (kOe)	$\Delta H_{k,2}$ (kOe)	σ (±0.25 kOe)
$Fe_{1-x}Cr_x$	0.020 ± 0.002	0.017	30 ± 1	20 ± 1	3.85
	0.054 ± 0.005	0.050	31 ± 1	22 ± 1	4.70
$Fe_{1-x}Mo_x$	0.012 ± 0.001	0.012	39 ± 1	26 ± 1	3.90
	0.031 ± 0.002	0.031	40 ± 1	27 ± 1	4.30
$Fe_{1-x}V_x$	0.003 ± 0.002	0.007	23.6 ± 0.5	23.6 ± 0.5	3.50
	0.014 ± 0.001	0.013	23.6 ± 0.5	23.6 ± 0.5	4.00

These evaluations are results from the deconvolution of the experimental spectra into some discrete subspectra. To check or improve these results, we have simulated the whole hyperfine-field distribution range, taking into account all of the surrounding shells, using steps of 4 kOe—bearing in mind that the first important precaution, before such a study is made, to ensure a valid evaluation, is the assurance of good homogeneity of all of the samples studied. That is why they were systematically tested by x-ray microprobe analysis.

In the first stage of the HFD simulation process, the field increments $\Delta H_{k,i}$ were varied for the mean composition values given by the x-ray microprobe analysis. In the last stage, for the increment values involving the minimum R-factor, the composition was varied down to the lowest R-value (see table 6).

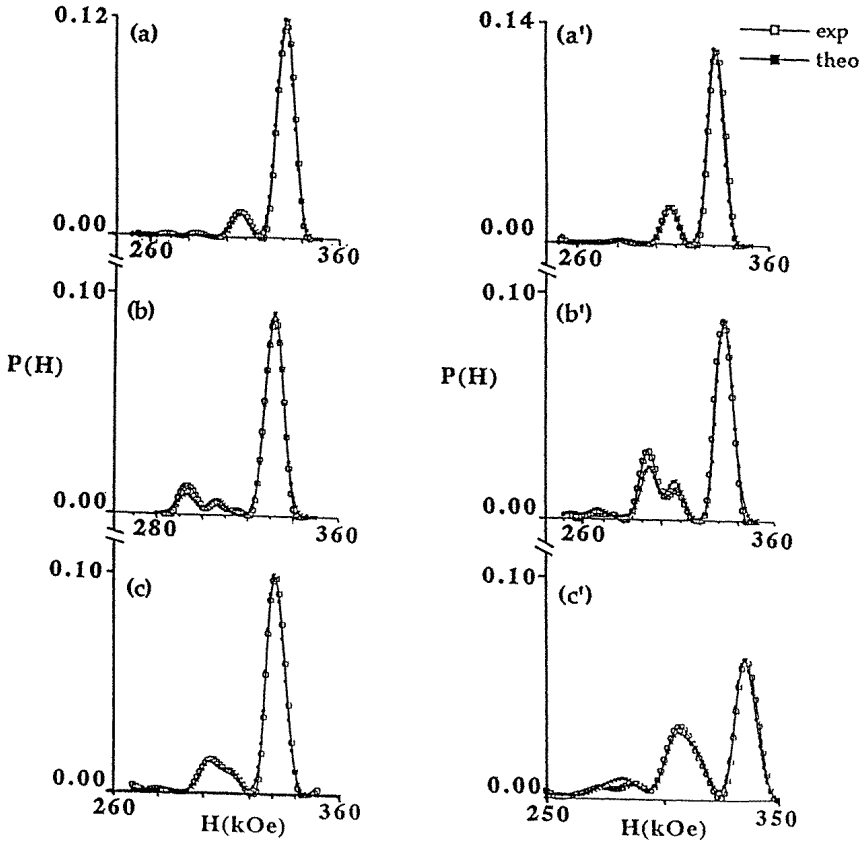

Figure 2. Hyperfine-field distributions (■: theoretical; □: experimental) at 300 K for the various $Fe_{1-x}M_x$ alloys (M = V, Mo, Cr) with x-values respectively equal to: (a) 0.007 ± 0.002; (a′) 0.013 ± 0.002 (M = V); (b) 0.012 ± 0.002; (b′) 0.031 ± 0.002 (M = Mo); (c) 0.017 ± 0.002; (c′) 0.050 ± 0.002 (M = Cr).

For the various binary alloy composition ranges covering the composition of the M50 steel with its possible evolution (figure 2), we corroborate the most pronounced effects of Mo incorporation: $\Delta H_{\mathrm{Mo},1} = -39 \pm 1$ kOe, $\Delta H_{\mathrm{Mo},2} = -26 \pm 2$ kOe. The disturbances caused by the first and second V neighbours for the Fe nuclei were found to be identical: $\Delta H_{\mathrm{V},1} = \Delta H_{\mathrm{V},2} = -24.0 \pm 0.5$ kOe. This is already suggested by the unique satellite peak in the HFD. We assess two different increment values for the Cr neighbours as illustrated by the two satellite peaks: $\Delta H_{\mathrm{Cr},1} = -30 \pm 1$ kOe, $\Delta H_{\mathrm{Cr},2} = -20 \pm 1$ kOe. The σ-value which takes into account the third- and higher-shell contributions increases, logically, when increasing x, from 3 kOe for the lowest x-value up to 5 kOe for $x = 0.05$. The comparison of these values with the values of the field increment shows that it would have no physical meaning to specify the field increments for each individual higher shell. It should be mentioned too that neither the quadrupole splitting (ε) nor the isomer shifts (δ)

appear specifically in the distribution curve, which relates only to the hyperfine magnetic field. This does not affect the composition determination, since the probabilities are studied over all of the detected magnetic field domain. Only the limitation of the study to a narrow field area would imply knowledge of the δ- and ε-values, but one must not forget that these hyperfine parameters are defined with very poor accuracy compared to the field values. The δ- and ε-effects would induce a broadening of some contributions to the hyperfine-field distribution, and might explain small discrepancies between the calculated and experimental $P(H)$ curves. However, some local heterogeneities in the atom distribution might also be responsible for these deviations. In fact, all of these effects are finally taken into account by the σ-parameter, which simulates any broadening of the individual lines.

As no clear statement has been given to date regarding the C increments, $\Delta H_{C,i}$, relative to the first and second interstitial neighbours of one Fe atom, we took into account the previous study by Cadeville *et al* on disordered splat-quenched FeC_x alloys with $x \leqslant 0.05$ [4]. These alloys were observed as a mixture of 'cubic massive and tetragonal martensites', but the authors concluded that the two kinds of phase were equivalent as regards their microscopic properties, as long as the local environment of the C atom is involved. The resistivity and hyperfine fields were not sensitive to the simultaneous presence of the two phases.

The relative abundance of the various subspectra resulting from the deconvolution of these splat-quenched alloy spectra up to $x = 0.05$ appear to be in perfect agreement with a statistical distribution of C atoms in the Fe lattice (see table 4). The Fe species assignment and therefore also the two increments $\Delta H_{C,i}$ are provided by the comparison between the experimental abundance of the subspectra and their theoretical probabilities calculated for the three Fe neighbourhoods associated with a statistical distribution of the C atoms on the octahedral sites O_c. Within the range of the experimental errors, the following field increments can be deduced:

$$\Delta H_{C,1} = -58 \pm 6 \text{ kOe}$$
$$\Delta H_{C,2} = +14 \pm 2 \text{ kOe}.$$

One must emphasize that, whether the phases are b.c.c. α or b.c.t. α', the important point is that the deformation of the octahedral sites be identical in the two cases. This allows the determination of the first- and second-C-neighbour disturbances, which can be used subsequently in the case of any martensite. The hyperfine fields assigned to Fe II and Fe III are respectively equal to $H(0) + \Delta H_{C,1}$ or $H(0) + \Delta H_{C,2}$ (272 ± 6 kOe and 344 ± 2 kOe), corroborating the validity of the additivity for low C contents. Although these $\Delta H_{C,i}$ increments are not obtained from the $P(H)$ simulations as for the substitutional elements, the values -58 and $+14$ kOe provide the correct order of magnitude for the $\Delta H_{C,i}$ parameters initiating the $P(H)$ martensite simulation procedure. In the last stage of the simulation, they were refined, limited by the uncertainties given above. It must be noted that Cadeville *et al* [4] have more indirectly assigned the various fields to the four equatorial and two axial possible C positions on the basis of the slopes of the curves representing the various subspectral abundances, as a function of the C content. The slope of the curve attributed to the Fe II species is twice that of the curve attributed to the Fe III species, as could be expected from the corresponding probabilities, or from the abundances reported in table 4. For all types of solute, the perfect agreements between the mean experimental field $\langle H_{exp} \rangle$ and the mean theoretical field $\langle H_{theo} \rangle$ confirm the reliability of the method, leading to, on the one hand, the field increments, and, on the other hand, the alloy compositions.

4.2. Structural study of the M50 steel in its annealed and quenched states

The M50 steel in its most complex state can be considered as a combination of the effects of substitution by three metallic atomic species and carbon interstitials. Moreover, up to now, no quantitative simulations of the hyperfine-field distributions have been performed. Consequently, it appeared essential to first define the steel structure in the ferritic state, where interstitial atoms can be neglected, and where the validity of the $P(H)$ simulation methodology can be more clearly tested. Furthermore, after quenching from various $\Theta\gamma$ temperatures, the fraction of metallic substitutional elements in the Fe matrix is known to increase in accordance with the carbide dissolution, so the ferrite (the annealed state) appears as the reference state, characterized by a lower substitution rate as compared to that for the quenched martensitic states. The superimposed effect of interstitial carbon complicates the analysis, and we must not forget the increase in the fraction of the substitutional element. That is why a study of the martensite will follow that of the ferrite.

4.2.1. Ferrite. The Mössbauer spectrum (figure 3) shows a broadened sextuplet consistent with the iron lattice substitution, and a paramagnetic peak of relative abundance equal to 4.8% for the whole spectrum, which is attributed to the Fe-substituted paramagnetic carbides [1]. The corresponding matrix hyperfine-field distribution $P(H)_{exp}$ (figure 4) exhibits, in addition to the main peak corresponding to undisturbed Fe neighbours, two satellite peaks relevant to the Fe neighbourhood disturbed mainly by the first and second solute neighbours. Their relative abundance of 30.7% is consistent with a solute content trapped within the matrix of 2.5 at.%, on the assumption of a statistical solute distribution.

Table 7. Compositions of the matrix $(Fe_{1-u-y-z}Cr_uMo_yV_z)C_x$ of the M50 steel for the ferrite F (the annealed state) and the martensite M, quenched from various temperatures.

	u(Cr)	y(Mo)	z(V)	x(C)	σ
F	0.017 ± 0.002	0.005 ± 0.002	0.003 ± 0.002	—	6 ± 0.3
M, 1273 K	0.049 ± 0.003	0.005 ± 0.002	0.003 ± 0.002	0.018 ± 0.004	7.5 ± 0.5
M, 1373 K	0.050 ± 0.003	0.010 ± 0.002	0.004 ± 0.002	0.025 ± 0.005	8 ± 0.5
M, 1423 K	0.053 ± 0.003	0.013 ± 0.002	0.005 ± 0.002	0.035 ± 0.005	8.5 ± 0.5

The best agreement between $P(H)_{exp}$ and the distribution simulation leads to different specific atomic contributions: 0.017 ± 0.002 Cr, 0.005 ± 0.002 Mo, 0.003 ± 0.001 V (see table 7, and figure 4). Compared to the nominal Cr, Mo, and V composition, these results assess the more important relative amount of Cr in the matrix, in agreement with its less pronounced effect on the carbide former. Just as for the binary alloys, the σ-parameter, which is equal to 6.0 ± 0.3 kOe, involves the effects of δ and ε on the higher shells. This value, close to those of the binary alloys, attests to the fraction of foreign atoms in this multi-component combination remaining in the same composition range as that for the binary alloys, and to the fact that the δ- and ε-disturbances are still small. The experimental crystalline parameter (a) of the ferrite was found to be equal to 0.2869 ± 0.0001 nm [11]. This small increase relative to the value for α-Fe is in agreement with the substitution for the Fe atom of bigger ones ($r_{Fe} = 0.124$ nm, $r_{Cr} = 0.125$ nm, $r_V = 0.132$ nm, $r_{Mo} = 0.136$ nm). Referring to the work of Bowman *et al* [12], we then refined the curve representing the bcc iron parameter (a) as a function of the Mo content (x) to a polynomial law:

$$a = -4.057 \times 10^{-5}x^2 + 35.196 \times 10^{-5}x + 0.286\,62.$$

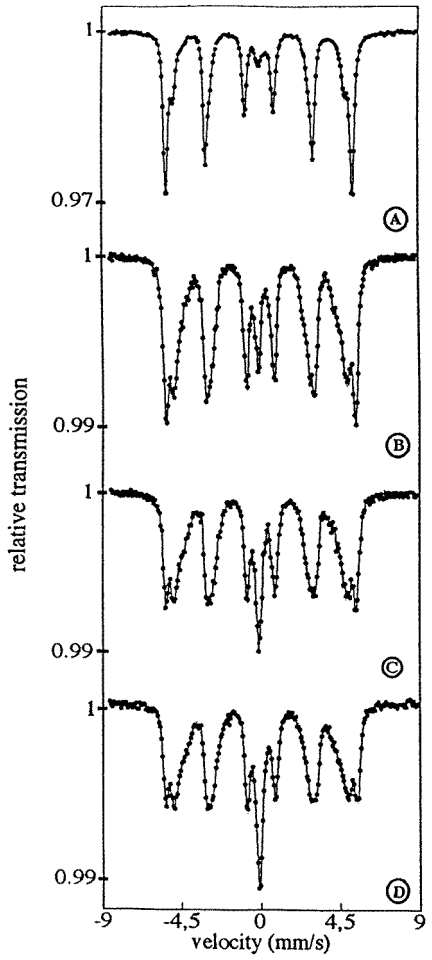

Figure 3. M50 steel Mössbauer spectra at 300 K (●: experimental points; ——: theoretical curve). (A) Ferrite. (B) Martensite after quenching from 1273 K. (C) Martensite after quenching from 1373 K. (D) Martensite after quenching from 1423 K.

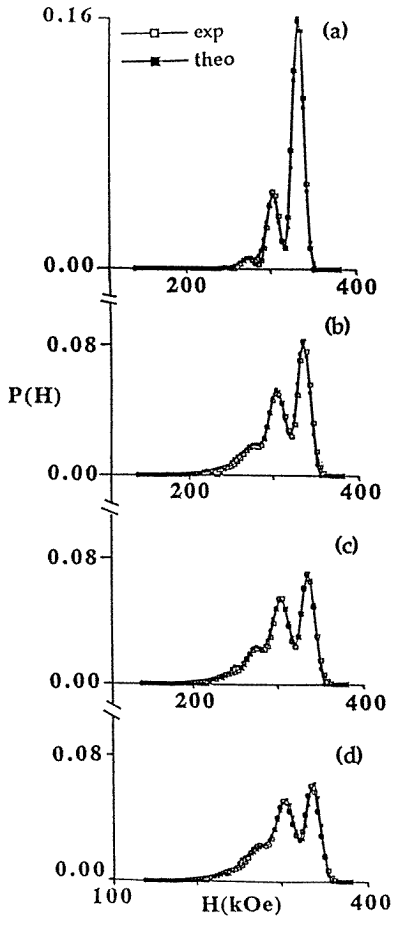

Figure 4. Hyperfine-field distributions at 300 K. (a) Ferrite. (b) Martensite after quenching from 1273 K. (c) Martensite after quenching from 1373 K. (d) Martensite after quenching from 1423 K.

For $a = 0.2869$ nm the calculated Mo content is found to be equal to 0.0088. With the approximations of a negligible influence of Cr atoms due to their quasi-similarity to the iron radii, and steric effects from V atoms approaching those of Mo, the sum of the V and Mo fractions substituted in the b.c.c. iron lattice (0.008) evaluated by Mössbauer spectroscopy accords perfectly with this crystallographic approach. Moreover, the resulting theoretical mean hyperfine field $\langle H_{theo} \rangle = 320 \pm 1$ kOe agrees with the mean experimental hyperfine field $\langle H_{exp} \rangle = 321 \pm 1$ kOe, giving additional support to our solute content determination.

4.2.2. Martensite. The gradual dissolution of the carbides as a function of the increasing austenizing temperature is responsible for the progressive enrichment of the matrix in solutes and carbon, as manifested by the broadening and the appearance of a shoulder exhibited by

the Mössbauer spectra (figure 3). Moreover, the central paramagnetic peak resulting from the residual austenite increases with the austenizing temperatures, while, at the same time, the Fe-substituted paramagnetic carbide contribution decreases [1].

Figure 4 reveals the on the whole excellent agreement between the calculated and experimental hyperfine-field distributions for all of the quenched samples. Unlike those for ferrite, the distributions $P(H)_{exp}$ for martensite are characterized by an increase in the upper-field-limit values to over 330 kOe, conforming with the perturbation $\Delta H_{C,2}$. The small discrepancies observed between $P(H)_{exp}$ and $P(H)_{cal}$, particularly in the low-field range, can be explained, as mentioned above, by either a small deviation from the multinomial law, or by the fact that δ and ε were included in a single σ-parameter.

We can justify our approach in several ways. As was evident in Cadeville's study, the most noticeable quadrupole splitting might be for the Fe III family, for which the contribution to the Mössbauer spectrum is, at most, 7% of the whole spectrum, for zero metallic substitution with a C content equal to 0.04. This perturbation, localized at around 272 kOe for zero alloying element, appears far below 272 kOe for the substituted Cr, Mo, V steel. It would be far-fetched to take into account such electrical perturbations localized in the $P(H)$ tail, where the experimental accuracy is at its lowest. Furthermore, the electric field gradients caused by the alloying elements depend on the relative atomic positions, and can compensate the electric field gradient from its first neighbour experienced by the Fe nucleus.

Table 7 makes it clear that, after the austenizing at 1373 K, Cr carbide dissolution is complete up to a Cr atomic content (u) equal to 0.053 ± 0.003. However, the slight difference from the nominal common commercial composition may just be for the specific commercial batch studied here. The Mo atomic content (y) in the matrix reaches 0.013 ± 0.003 at 1423 K, in relation with the Mo carbide dissolution which starts at 1273 K for M_6C and at 1373 K for M_2C. From 1273 K up to 1423 K, the V content (z) appears quasi-constant, owing to its low value. The concomitant C insertion (x), equal to 0.035 ± 0.005 at 1423 K determined from the 1423 K quenched spectrum, lies near to the nominal C content ($x = 0.04$).

These results are corroborated by x-ray diffraction studies and a scanning transmission electron microscopy determination [11]. It appears that at 1273 K the majority of the Cr is dissolved into the matrix. Taking into account the main metallic component M of a given carbide, the x-ray diffraction patterns show that $(Fe–M)_{23}C_6$ (M = Cr) is completely dissolved into the matrix, while $(Fe–M)_7C_3$ (M=Cr) is not yet dissolved. At 1373 K, the dissolution of $(Fe–M)_6C$ (M = Mo) is in progress, and the matrix becomes partially Mo enriched. At the same time, the content of C inserted into the matrix increases. At 1423 K, the matrix continues to be slightly enriched in Mo, V, and C, due to the gradual dissolution of $(Fe–M)_2C$ (M = Mo and V) initiated at 1273 K.

5. Conclusion

In this paper, a method has been developed, involving Mössbauer spectroscopy, which provides a detailed understanding of a given steel, and may later monitor any transformation. From the hyperfine-field distribution $P(H)$, the natures and fractions of atomic elements dispersed in the Fe ferromagnetic matrix, either at substitutional or interstitial sites, are defined. Whatever the values of δ and ε, each individual site is detected from its appropriate hyperfine field, centred on a gaussian line, broadened by δ- and ε-effects, and interactions with higher shells, which are small compared to the magnetic field disturbances. If any ambiguity appears among the atomic surroundings in such multi-component systems, in a particular magnetic field area of the $P(H)$ distribution, all doubts about the alloy

composition can be removed using the knowledge of $P(H)$ values obtained in other areas, since the analysis was performed throughout the magnetic hyperfine-field domain. This method can be applied whenever the atomic fraction of each individual element k is in the low-dilution range (<0.05), as long as the steel can be considered as a disordered system, obeying the multinomial law, with the assumption of independent and additive perturbations introduced by the foreign atoms into the Fe local hyperfine field. Only neutron diffraction can localize such different elements. However, Mössbauer spectroscopy can be more easily implemented. In the special case of the M50 steel, after accurate determination of each alloying element perturbation, it has been possible to obtain the quantities of Cr, Mo, and V atoms substituted in the Fe lattice of the ferrite (the annealed state), the remaining fraction being combined in the carbides. This most simple state stands as a reference state for our analysis, compared to the more complex case of quenched martensite. In the latter case, the fraction of foreign elements trapped in the ferromagnetic matrix increases to conform with the gradual dissolution of the numerous carbides. The maximum fraction of Cr, Mo, V, and C atoms specifically detected in the present study is reached for an austenizing temperature of 1423 K if abnormal grain growth is to be avoided. The same analysis could be performed on tempered martensite in order to follow up the secondary hardening.

References

[1] Decaudin B, Djega-Mariadassou C and Cizeron G 1995 *J. Alloys Compounds* **226** 208
[2] Djega-Mariadassou C, Bessais L and Servant C 1995 *Phys. Rev.* B **51** 8830
[3] Le Caer G and Dubois J M 1979 *J. Phys. E: Sci. Instrum.* **12** 1083
[4] Cadeville M C, Friedt J M and Lerner C 1977 *J. Phys. F: Met. Phys.* **7** 123
[5] Vincze I and Campbell I A 1973 *J. Phys. F: Met. Phys.* **3** 654
[6] Wertheim G K, Jaccarino V, Wernick J H and Buchanan D N E 1964 *Phys. Rev. Lett.* **12** 24
[7] Cranshaw T E, Johnson C E, Ridout M S and Murray G A 1966 *Phys. Lett.* **21** 481
[8] Cranshaw T E 1972 *J. Phys. F: Met. Phys.* **2** 615
[9] Dean R H, Furley R J and Scurlock R G 1964 *J. Physique* **25** 596
[10] Asano A and Schwartz L H 1973 *AIP Conf. Proc.* **18** 262
[11] Decaudin B 1995 *Thèse de l'Université Paris-Sud*
[12] Bowman F E, Park R M and Herzig A J 1943 *Trans. ASME* **6** 487